

Accepted Manuscript

Glycosylated tris-bipyridine ferrous complexes for probing a mechanism behind carbohydrate-carbohydrate interactions: Spatial carbohydrate packing of glycoclusters changes on additions of salts in carbohydrate- and anion-dependent manners

Naoto Chigira, Fumiko Dai, Yuki Nonaka, Koki Sato, Yoshitsugu Amano, Maki Sekiguchi, Mayu Inokuchi, Masahito Hagio, Teruaki Hasegawa

PII: S0040-4020(18)30970-0

DOI: [10.1016/j.tet.2018.08.017](https://doi.org/10.1016/j.tet.2018.08.017)

Reference: TET 29737

To appear in: *Tetrahedron*

Received Date: 14 June 2018

Revised Date: 24 July 2018

Accepted Date: 13 August 2018

Please cite this article as: Chigira N, Dai F, Nonaka Y, Sato K, Amano Y, Sekiguchi M, Inokuchi M, Hagio M, Hasegawa T, Glycosylated tris-bipyridine ferrous complexes for probing a mechanism behind carbohydrate-carbohydrate interactions: Spatial carbohydrate packing of glycoclusters changes on additions of salts in carbohydrate- and anion-dependent manners, *Tetrahedron* (2018), doi: 10.1016/j.tet.2018.08.017.

This is a PDF file of an unedited manuscript that has been accepted for publication. As a service to our customers we are providing this early version of the manuscript. The manuscript will undergo copyediting, typesetting, and review of the resulting proof before it is published in its final form. Please note that during the production process errors may be discovered which could affect the content, and all legal disclaimers that apply to the journal pertain.



Graphical Abstract

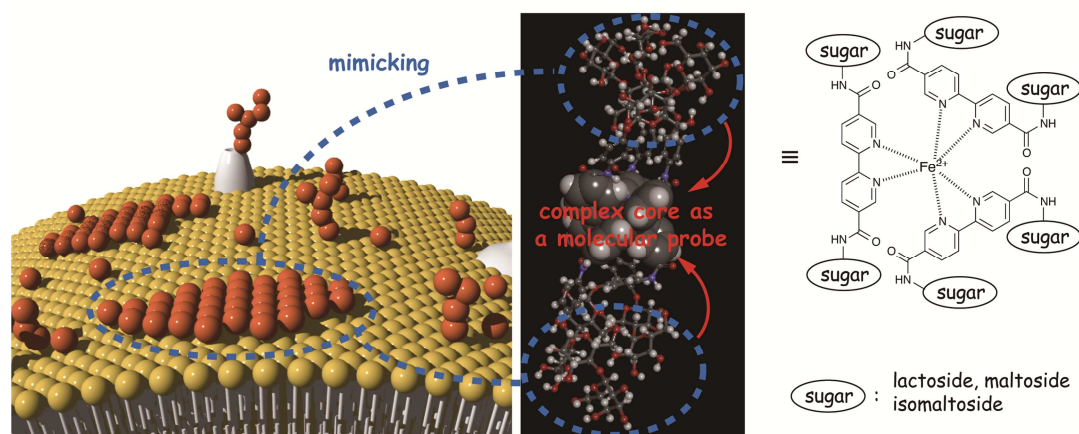
Glycosylated tris-bipyridine ferrous complexes for probing a mechanism behind carbohydrate-carbohydrate interactions: spatial carbohydrate packing of glycoclusters changes on additions of salts in carbohydrate- and anion-dependent manners

Naoto Chigira^{a,§}, Fumiko Dai^{a,§}, Yuki Nonaka^a, Koki Sato^b, Yoshitsugu Amano^a, Maki Sekiguchi^b, Mayu Inokuchi^b, Masahito Hagio^b and Teruaki Hasegawa^{b,c,*}

^aGraduate School of Life Sciences, Toyo University, 1-1-1 Izumino, Itakura-machi, Ora-gun, Gumma 374-0193, Japan, ^bFaculty of Life Sciences, Toyo University, 1-1-1 Izumino, Itakura-machi, Ora-gun, Gumma 374-0193, Japan, ^cBio-Nano Electronics Research Centre, Toyo University, 2100 Kujirai, Kawagoe, Saitama 350-8585, Japan.

[§]These two authors contributed equally to this work.

Leave this area blank for abstract info.





Glycosylated tris-bipyridine ferrous complexes for probing a mechanism behind carbohydrate-carbohydrate interactions: spatial carbohydrate packing of glycoclusters changes on additions of salts in carbohydrate- and anion-dependent manners

Naoto Chigira^{a, §}, Fumiko Dai^{a, §}, Yuki Nonaka^a, Koki Sato^b, Yoshitsugu Amano^a, Maki Sekiguchi^b, Mayu Inokuchi^b, Masahito Hagio^b and Teruaki Hasegawa^{b, c, *}

^aGraduate School of Life Sciences, Toyo University, 1-1-1 Izumino, Itakura-machi, Ora-gun 374-0193, Japan

^bFaculty of Life Sciences, Toyo University, 1-1-1 Izumino, Itakura-machi, Ora-gun 374-0193, Japan

^cBio-Nano Electronics Research Centre, Toyo University, 2100 Kujirai, Kawagoe 350-8585, Japan

[§]These two authors contributed equally to this work

*Corresponding author

E-mail address: t-hasegawa@toyo.jp

ARTICLE INFO

Article history:

Received

Received in revised form

Accepted

Available online

Keywords:

carbohydrate-carbohydrate interactions

tris-bipyridine ferrous complex

glycocluster

dynamic combinatorial library

circular dichroism

spatial carbohydrate packing

ABSTRACT

2,2'-Bipyridines containing two β -maltoside, β -lactoside, or β -isomaltoside appendages were prepared and successively complexed with ferrous ion to afford hexavalent glycoclusters having tris-bipyridine ferrous complex cores. Each of these metalloglycoclusters showed unique UV-vis and CD spectral changes upon addition of chlorides, nitrates, and sulfate salts in carbohydrate- and anion-dependent manners. The results indicate that spatial carbohydrate packing of the metalloglycoclusters changes upon addition of these anions and that different anions stabilize different carbohydrate packings. Furthermore, the sulfates specifically enhance the rheological properties of aqueous solutions containing the metalloglycocluster containing β -lactoside appendages.

2018 Elsevier Ltd. All rights reserved.

1. Introduction

Glycosphingolipids (GSLs) in cell membranes aggregate laterally to form GSL-enriched microdomains presenting densely packed carbohydrate clusters (glycoclusters) on cell surfaces (Fig. 1-a).¹⁻³ It has been reported that these cell surface glycoclusters play essential roles in cell-cell adhesion via carbohydrate-carbohydrate interactions (CCIs), wherein GSLs on the surface of one cell recognize GSLs on the surface of an adjacent cell in specific, multivalent, and, in some cases, Ca^{2+} -dependent manners.⁴ For example, Le^X - Le^X and G_M3 - G_G3 interactions were reported to induce compaction of blastomeres and migration of cancer cells, respectively.^{5,6} Since cell-cell adhesion is a fundamental bioprocess in multicellular organisms, investigation into CCIs is of quite high importance from an academic viewpoint. It is also an attractive research topic for industry, since novel knowledge will support the design of new drugs for the prevention of various diseases triggered by unfavorable cell-cell adhesions (metastases, inflammations, etc.). In spite of the importance of CCIs, the fluidic nature of cell membranes as well as dynamic fluctuations in their GSL levels make it quite difficult to investigate CCIs in a detailed manner. In fact, very little molecular-level information about CCIs has been obtained thus far. In particular, no information is available

concerning the conformation (spatial packing of the carbohydrate units) in glycoclusters.

The weakness of CCIs further compounds the difficulty in their investigation; a single CCI between two isolated carbohydrates is too weak to be detected. Well-designed artificial systems are thus vital in this research field⁷⁻²²; such artificial systems may contain synthetic polymers,⁸ peptides,^{9,10} foldamers,¹¹ cyclodextrins,¹² and liposomes,¹³⁻¹⁵ all having multiple carbohydrate appendages. Gold nanoparticles (GNPs) coated with densely packed glycoclusters are also well-known model systems for probing CCIs.¹⁶⁻¹⁸ For example, Le^X - Le^X interactions were successfully probed through Ca^{2+} -mediated aggregation of GNPs carrying multiple Le^X -trisaccharides (Le^X_3 ; $\text{Gal}\beta 1,4(\text{Fuc}\alpha 1,3)\text{GlcNAc}\beta$).¹⁸ Dendrimers having multiple lactosides (Lac; $\text{Gal}\beta 1,4\text{Glc}\beta$) and lipid monolayers containing G_M3 ($\text{NeuAc}\alpha 2,3\text{Gal}\beta 1,4\text{Glc}\beta$) were also useful for probing G_M3 -Lac interactions at an air-water interface.¹⁹ Lac-Lac interactions were also successfully probed using a polyfluorene with multiple Lac appendages; Ca^{2+} mediated association of the Lac-appended polyfluorene more efficiently than did K^+ , Na^+ , Mg^{2+} , or Ba^{2+} .²⁰ As these previous researches have exemplified, researchers in this field commonly believe that the ions function as a molecular glue to join two carbohydrate units together, and that formation of multiple carbohydrate-ion-carbohydrate

complexes is a main driving force mediating the CCI. However, no attention has been paid to the spatial carbohydrate packings within these glycoclusters.

We have also developed various model systems for probing CCIs.²³⁻²⁶ Recently, we developed tris-bipyridine (tris-bpy) ferrous complex having six Lac appendages ($[\text{Fe}(\text{bpy})\text{Lac}]_3^{2+}$) and the same having six maltoside (Mal; $\text{Glc}\alpha 1,4\text{Glc}\beta$) appendages ($[\text{Fe}(\text{bpyMal})_3]^{2+}$).²⁶ Each of these metalloglycoclusters exists as a mixture of two diastereomers (Δ and Λ) with different carbohydrate packings (Fig. S1). Their Δ - and Λ - $[\text{Fe}(\text{bpy})_3]^{2+}$ cores have screw-propeller-like 3D structures, in which three bpy units coordinate the Fe^{2+} in right- and left-handed manners, respectively. Since the N-Fe bonds are reversible at ambient temperature, the two diastereomers are under dynamic equilibrium, in which the Δ - Λ ratio changes depending on their relative stabilities (Fig. S2). Molecular dynamics (MD) simulations revealed that these metalloglycoclusters have unique 3D structures in which two trivalent glycoclusters are positioned at the northern and southern poles of the spherical $[\text{Fe}(\text{bpy})_3]^{2+}$ cores (Fig. 1-b). Each of these trivalent glycoclusters would mimic the natural glycoclusters on cell surfaces. An advantage of the metalloglycoclusters created by our group is that the $[\text{Fe}(\text{bpy})_3]^{2+}$ cores, which act as molecular probes, are located in close proximity to the trivalent glycoclusters. Since the trivalent glycoclusters are energetically coupled with the $[\text{Fe}(\text{bpy})_3]^{2+}$ cores, ion-induced conformational changes in the former can be readily monitored by the Δ - Λ ratio of the latter. Using such model systems, we investigated carbohydrate packings in the systems both with and without ions, and found that various ions including Na^+ , K^+ , Mg^{2+} , Ca^{2+} , and Cl^- bind to the glycoclusters and greatly change their carbohydrate packing in both carbohydrate- and ion-dependent manners. It should be noted that Lac is the carbohydrate unit of lactosylceramide (LacCer), which is one of major GSLs in cell membranes as well as a common structural motif of various GSLs (e.g., GM3 and Gg3). This finding is interesting since it suggests a mechanism behind CCI, which is that the ions make the carbohydrate packings suitable for the CCI and that the resultant glycoclusters smoothly interact with other glycoclusters intercellularly.

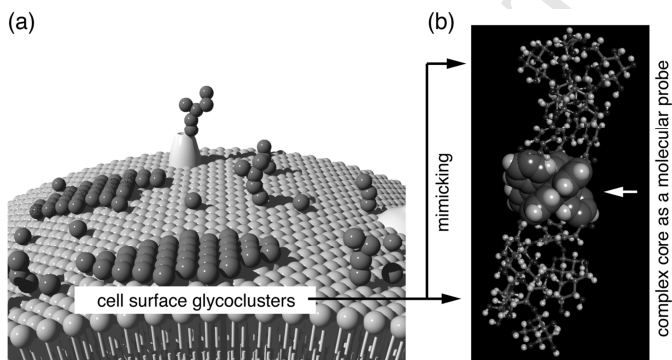


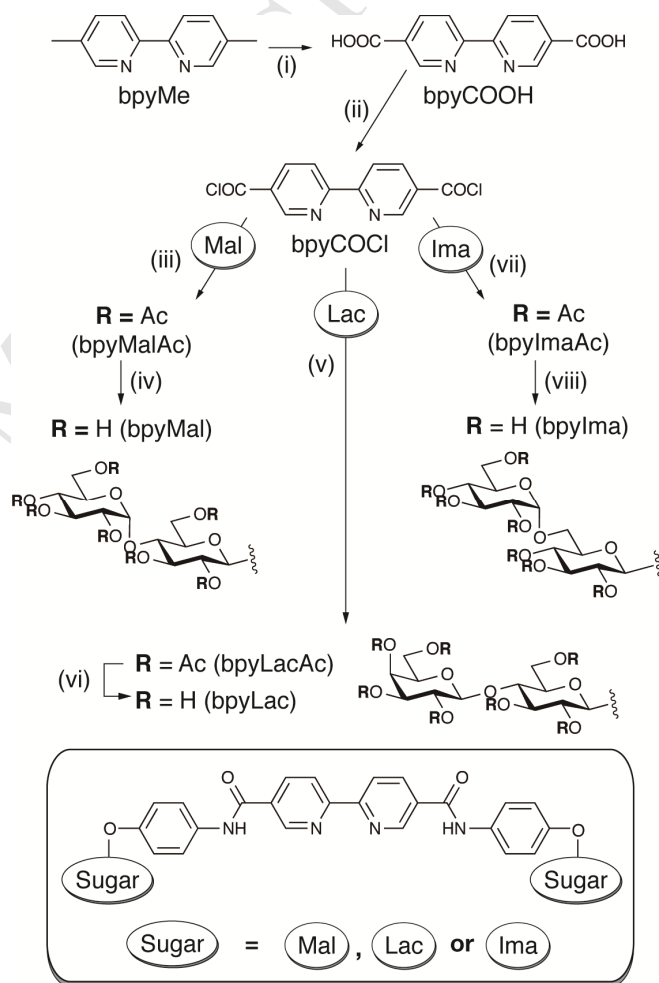
Fig. 1 (a) Illustration of glycoclusters on a cell surface and (b) the most stable conformation of Δ - $[\text{Fe}(\text{bpyLac})_3]^{2+}$ during the MD simulations (See Fig. S3 for the colored version of this figure).

In our previous paper, attention was primarily given to the effects of cations on the spatial carbohydrate packings, since it is widely believed that the cations (Ca^{2+} in some cases) play important roles in CCIs. However, in our further studies it was revealed that anions also have a great impact on spatial carbohydrate packings. We herein report novel experimental data concerning the ability of the anions to change spatial carbohydrate packings, and preliminary data concerning intermolecular CCIs between metalloglycoclusters.

2. Results and Discussion

2.1. Syntheses of glycosylated bipyridines (glycobpys)

Commercially available 5,5'-dimethyl-2,2'-bipyridine was oxidized with KMnO_4 in boiling water, and the resultant 2,2'-bipyridine-5,5'-dicarboxylic acid (bpyCOOH) was then converted into 2,2'-bipyridine-5,5'-dicarboxyl chloride (bpyCOCl) by SOCl_2 (Scheme 1). The coupling of bpyCOCl with *per-O*-acetyl-*p*-aminophenyl- β -maltoside (*p*APMal), *per-O*-acetyl-*p*-aminophenyl- β -lactoside (*p*APLac), and *per-O*-acetyl-*p*-aminophenyl- β -isomaltoside (*p*APIma) was followed by deacetylation to afford bpy having two lactoside (bpyLac), maltoside (bpyMal), or isomaltoside (bpyIma) appendages, respectively. Here, isomaltoside (Ima; $\text{Glc}\alpha 1,6\text{Glc}\beta$) is a structural isomer of Mal, and differs from Mal only in its glycosidic linkages. The synthesis of bpyIma is reported for the first time in this work and its detailed synthetic procedure and characterization are reported, while those of bpyMal and bpyLac were reported in our previous work.²⁶



Scheme 1 Reaction conditions: i) KMnO_4 , water, reflux, overnight, 74%, ii) SOCl_2 , reflux, 5 h, quant., iii) *p*APMal, Et_3N , THF, rt, 20 min, 46%, vi) aqueous ammonia, MeOH, rt, 3 days, quant., v) *p*APLac, Et_3N , THF, rt, 5 min, 36%, vi) aqueous ammonia, MeOH, rt, overnight, quant., vii) *p*APIma, Et_3N , THF, rt, 20 min, 61%, viii) aqueous ammonia, MeOH, rt, overnight, quant..

2.2. Preparation of tris-bipyridine ferrous complexes having six carbohydrate appendages

Usually, bpy derivatives are readily converted to the corresponding tris-bipyridine ferrous complexes in quantitative

yields by mixing them with a one-third molar equivalent of Fe^{2+} bound to $[\text{Fe}(\text{bpyMal})_3]^{2+}$ and induced its UV-vis spectral response. However, water solubility of the synthesized glycobpys was so low that their simple complexation with Fe^{2+} was not accomplished. In fact, repeated heating/sonication processes with 3 molar equivalents of Fe^{2+} were required for their complexation. The resultant solutions were radish purple in color without any precipitates, indicating successful and quantitative conversion of bpyMal, bpyLac, and bpyIma into $[\text{Fe}(\text{bpyMal})_3]^{2+}$, $[\text{Fe}(\text{bpyLac})_3]^{2+}$, and $[\text{Fe}(\text{bpyIma})_3]^{2+}$, respectively. Even in the presence of excess amounts of Fe^{2+} , the metalloglycoclusters having $[\text{Fe}(\text{bpy})_3]^{2+}$ cores were formed exclusively, as determined from their strong metal-to-ligand charge transfer (MLCT) UV-vis bands at ~ 575 nm (Fig. S4).

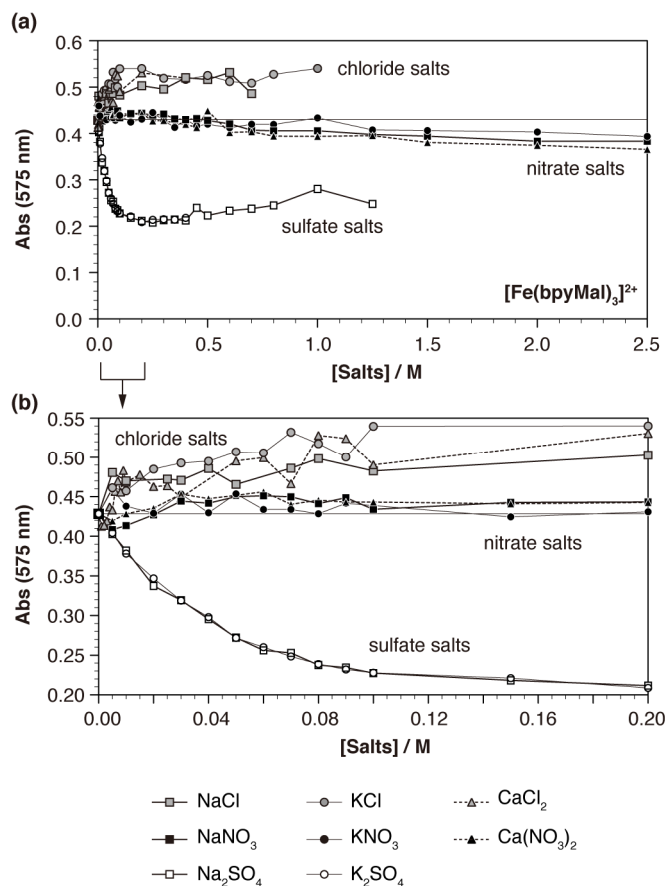


Fig. 2 (a) MLCT intensity of $[\text{Fe}(\text{bpyMal})_3]^{2+}$ in the presence of various concentrations of salts and (b) an enlarged version. $[\text{bpyMal}] = 2.44$ mM, $[\text{FeCl}_2] = 7.33$ mM, $d = 0.2$ mm, rt, in water.

2.3. Salt-induced UV-vis spectral changes of the metalloglycoclusters

2.3.1. Salt-induced UV-vis spectral changes of $[\text{Fe}(\text{bpyMal})_3]^{2+}$

The metalloglycoclusters showed unique UV-vis spectral responses toward chloride (NaCl , KCl , and CaCl_2), nitrate (NaNO_3 , KNO_3 , and $\text{Ca}(\text{NO}_3)_2$), and sulfate salts (Na_2SO_4 and K_2SO_4) (Fig. S4). For example, in the case of $[\text{Fe}(\text{bpyMal})_3]^{2+}$, the intensity of its MLCT band clearly increased in the presence of the chloride salts (Fig. 2, gray symbols). In contrast, the sulfate salts exhibited different effects, drastically decreasing the MLCT intensity upon their addition (Fig. 2, white symbols). Note that in both groups (the chloride and the sulfate salts), little difference was induced in the UV-vis spectral response by the different cations, indicating that their anions (Cl^- and SO_4^{2-})

bound to $[\text{Fe}(\text{bpyMal})_3]^{2+}$ and induced its UV-vis spectral response.

In contrast to the clear UV-vis spectral changes induced by the chloride and sulfate salts, the nitrate salts induced only negligible UV-vis spectral changes (Fig. 2, black symbols). However, it should be noted that these negligible UV-vis spectral changes does not signify that no affinity exists between the nitrates and $[\text{Fe}(\text{bpyMal})_3]^{2+}$. On the contrary, their binding was clearly demonstrated via circular dichroism (CD) spectroscopy measurements, as discussed in section 2.4.

2.3.2. Salt-induced UV-vis spectral changes of $[\text{Fe}(\text{bpyLac})_3]^{2+}$

The salt-induced UV-vis spectral changes of $[\text{Fe}(\text{bpyLac})_3]^{2+}$ were clearly different from those of $[\text{Fe}(\text{bpyMal})_3]^{2+}$. In the case of the chloride salts, $[\text{Fe}(\text{bpyLac})_3]^{2+}$ showed negligible UV-vis spectral changes, in clear contrast to the enhanced MLCT intensity induced in $[\text{Fe}(\text{bpyMal})_3]^{2+}$ (Fig. 3, gray symbols). Different UV-vis spectral responses between $[\text{Fe}(\text{bpyMal})_3]^{2+}$ and $[\text{Fe}(\text{bpyLac})_3]^{2+}$ were also observed for the sulfate salts (Fig. 3, white symbols). In this case, the MLCT intensity of $[\text{Fe}(\text{bpyLac})_3]^{2+}$ decreased with increasing sulfate salt concentration, falling nearly to zero when sulfate salt concentration was increased to ~ 0.3 M. In contrast to what was observed for $[\text{Fe}(\text{bpyLac})_3]^{2+}$, $[\text{Fe}(\text{bpyMal})_3]^{2+}$ still retained substantial MLCT intensity ($I/I_0 = 0.5-0.6$) even under much higher sulfate-concentrations (e.g., $[\text{Na}_2\text{SO}_4] = 1.25$ M, See section 2.3.1).

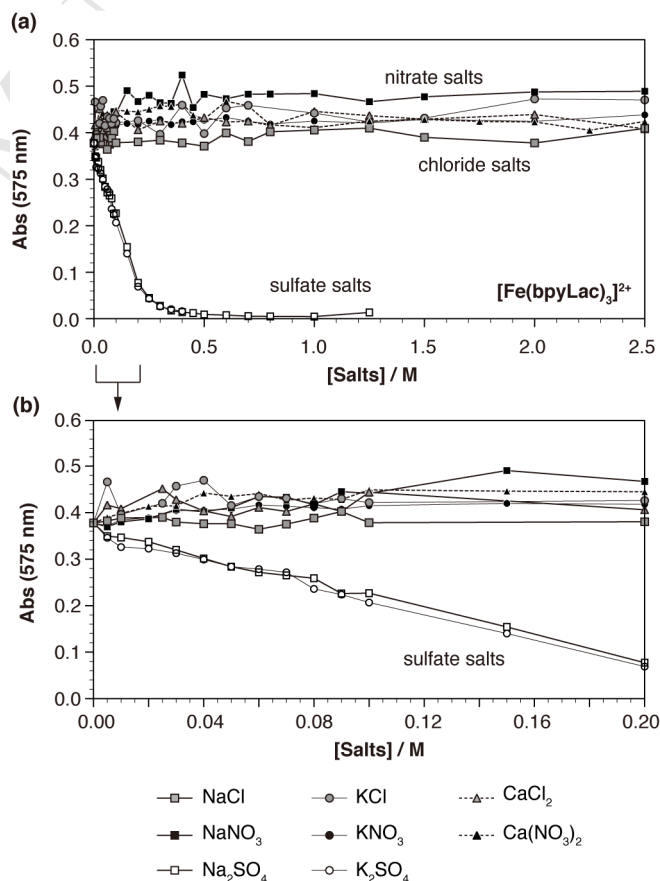


Fig. 3 (a) MLCT intensity of $[\text{Fe}(\text{bpyLac})_3]^{2+}$ in the presence of various concentrations of the salts and (b) an enlarged version. $[\text{bpyLac}] = 2.44$ mM, $[\text{FeCl}_2] = 7.33$ mM, $d = 0.2$ mm, rt, in water.

2.3.3. Salt-induced UV-vis spectral changes of $[\text{Fe}(\text{bpyIma})_3]^{2+}$

We also observed unique salt-induced UV-vis spectral responses of $[\text{Fe}(\text{bpyIma})_3]^{2+}$ which differed from those of both

$[\text{Fe}(\text{bpyMal})_3]^{2+}$ and $[\text{Fe}(\text{bpyLac})_3]^{2+}$. The most interesting data were obtained for the sulfate salts, which induced negligible UV-vis spectral changes in $[\text{Fe}(\text{bpyIma})_3]^{2+}$ (Fig. 4, white symbols). This is in clear contrast to the decreased MLCT intensity observed for $[\text{Fe}(\text{bpyMal})_3]^{2+}$ and $[\text{Fe}(\text{bpyLac})_3]^{2+}$ in the presence of the sulfate salts. The negligible UV-vis spectral changes provide strong evidence of the stability of the $[\text{Fe}(\text{bpy})_3]^{2+}$ cores in the presence of these sulfate salts.

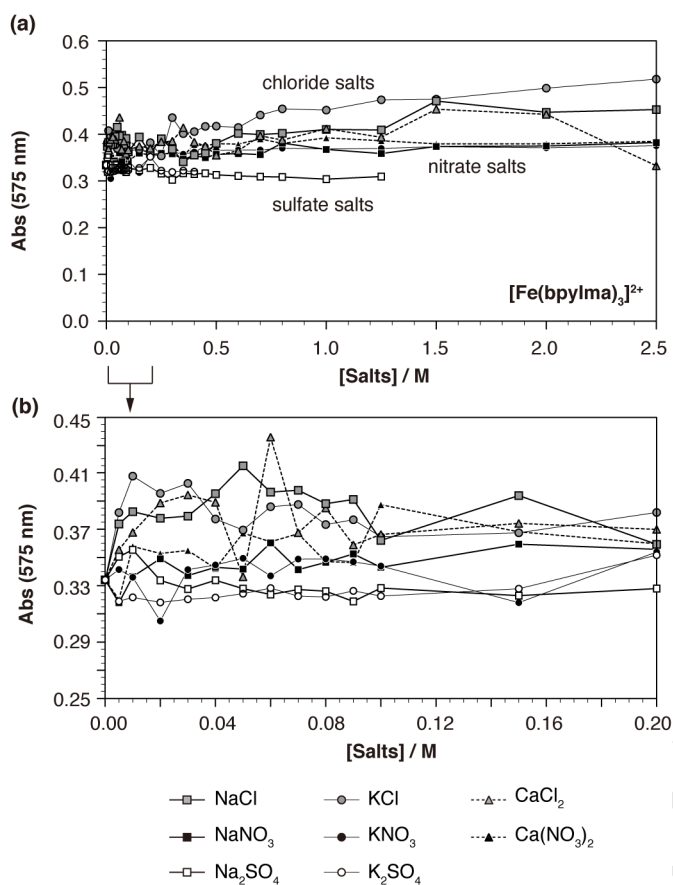


Fig. 4 (a) MLCT intensity of $[\text{Fe}(\text{bpyMal})_3]^{2+}$ in the presence of various concentrations of the salts and (b) an enlarged version. $[\text{bpyMal}] = 2.44 \text{ mM}$, $[\text{FeCl}_2] = 7.33 \text{ mM}$, $d = 0.2 \text{ mm}$, rt, in water.

2.4. Circular dichroism (CD) spectral changes of the metalloglycoclusters

2.4.1. Salt-induced CD spectral changes of $[\text{Fe}(\text{bpyMal})_3]^{2+}$

In the absence of salts, $[\text{Fe}(\text{bpyMal})_3]^{2+}$ exhibited a negative-to-positive CD pattern, as measured from longer to shorter wavelengths, centered around 315 nm (Fig. 5-a, bold line). This CD pattern resembles that reported for enantio-pure Δ - $[\text{Fe}(\text{bpy})_3]^{2+}$, indicating that $[\text{Fe}(\text{bpyMal})_3]^{2+}$ predominantly exists in its Δ form in pure water.²⁷ However, the signal intensities of $[\text{Fe}(\text{bpyMal})_3]^{2+}$ were much weaker in comparison to those of enantio-pure Δ - $[\text{Fe}(\text{bpy})_3]^{2+}$, indicating its low diastereomeric excess. This data indicates that the glycoclusters of $[\text{Fe}(\text{bpyMal})_3]^{2+}$ have flexible packings and that both diastereomers (Δ and Λ) have similar stabilities.

The addition of salts greatly changed the CD spectrum of $[\text{Fe}(\text{bpyMal})_3]^{2+}$. For example, the addition of chloride salts markedly enhanced the CD signal (Figs. 5-a and -b, gray symbols). Again, negligible differences were observed between the chloride salts of different cations (NaCl, KCl, and CaCl₂), suggesting that Cl⁻ is responsible for the CD spectral responses. The enhanced CD signal indicate that Cl⁻ changed the carbohydrate packing of the Mal clusters into a more rigid

packing suitable for the Δ - $[\text{Fe}(\text{bpy})_3]^{2+}$ core. This Cl⁻-induced conformational change of $[\text{Fe}(\text{bpyMal})_3]^{2+}$ was discussed in detail in our preceding work, in which it was assumed that multiple electrostatic interactions stemmed from the amide linkages ($-\text{NHCO}-$) in $[\text{Fe}(\text{bpyMal})_3]^{2+}$ are responsible for the Cl⁻-binding.²⁶

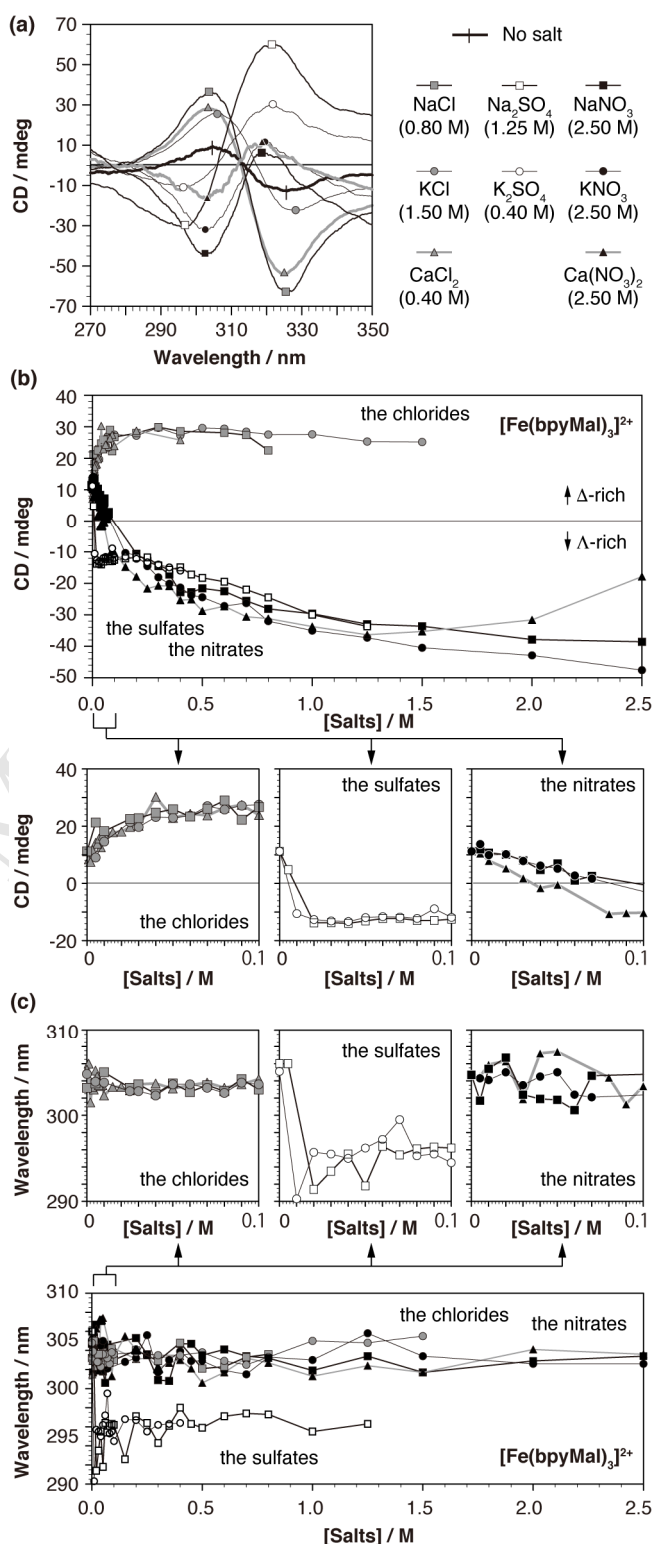


Fig. 5 (a) CD spectra of $[\text{Fe}(\text{bpyMal})_3]^{2+}$ with and without various salts, (b) plots of the intensity of the CD peak at the shorter wavelength (the left-most peaks in (a)) against salt concentration, and (c) wavelength of the CD peak at the shorter wavelength against salt concentration. $[\text{bpyMal}] = 2.44 \text{ mM}$, $[\text{FeCl}_2] = 7.33 \text{ mM}$, $d = 0.2 \text{ mm}$, rt, in water.

The negative-to-positive CD pattern of $[\text{Fe}(\text{bpyMal})_3]^{2+}$ in pure water was inverted, becoming positive-to-negative (when scanned from longer to shorter wavelengths) upon addition of the

sulfate or nitrate salts (Figs. 5-a and -b, white and black symbols, respectively). This data indicates that Λ -[Fe(bpyMal)₃]²⁺ became predominant upon addition of these salts. This observation is quite interesting since it means that different salts stabilize different carbohydrate packings (where chlorides stabilize different packings than sulfates and nitrates; Table 1). Again, the anions are responsible for the salt-induced CD spectral changes.

Although both the sulfate and the nitrate salts stabilized Λ -[Fe(bpyMal)₃]²⁺, they showed different concentration dependences. For example, in the case of the sulfate salts, relatively low concentrations were sufficient to induce the CD spectral inversion; the original negative-to-positive CD pattern was changed to a positive-to-negative pattern when sulfate salt concentrations were higher than 10–20 mM (Fig. 5-b, white symbols). The nitrate salts also induced similar CD spectral changes, but much higher concentrations (50–100 mM) were required to induce the CD spectral inversion (Fig. 5-b, black symbols), indicating that [Fe(bpyMal)₃]²⁺ has a stronger affinity to SO₄²⁻ than to NO₃⁻.

Along with the unique CD spectral changes, peak shifts of the CD signals were also induced upon addition of certain salts. For example, upon the addition of sulfate salts, the positive peak at ~304 nm was clearly blue-shifted to ~295 nm (Fig. 5-c, white symbols). Again, significant peak shifts were not observed between the solutions containing different cations, indicating that SO₄²⁻ was responsible for the blue shift. Interestingly, neither nitrate nor chloride salts induced shifts of the CD signal peak (Fig. 5-c, black and gray symbols, respectively).

Table 1 Diastereomeric excesses of the glycosylated tris-bipyridine ferrous complexes induced by the different salts^a

	No salt	Chloride salts	Sulfate salts	Nitrate salts
[Fe(bpyMal) ₃] ²⁺	Δ	$\Delta\Delta$	$\Lambda\Lambda$	$\Lambda\Lambda$
[Fe(bpyLac) ₃] ²⁺	Δ	$\Delta\Delta$	Δ	Δ ($\Delta\Delta$) ^b
[Fe(bpyIma) ₃] ²⁺	Δ	$\Lambda\Lambda$	- ^c	$\Delta\Delta$

^a Δ indicates that the Δ isomer dominated in a low diastereomeric excess, while $\Delta\Delta$ indicates an amplified diastereomeric excess. ^b $\Delta\Delta$ only for NaNO₃ (1–300 mM). ^cStable diastereomers could not be clarified, since the resultant CD spectra were entirely different from those of Δ - and Λ -[Fe(bpy)₃]²⁺.

2.4.2. Salt-induced CD spectral changes of [Fe(bpyLac)₃]²⁺

In the absence of salts, [Fe(bpyLac)₃]²⁺ showed a negative-to-positive CD pattern of weak intensity, as measured from longer to shorter wavelengths, centered around 315 nm. Its CD spectrum was quite similar to that of [Fe(bpyMal)₃]²⁺, indicating that the glycoclusters of [Fe(bpyLac)₃]²⁺ also have a flexible packing in pure water.

Before beginning a discussion of the CD spectral responses of [Fe(bpyLac)₃]²⁺ towards the salts, the most conceivable mechanism of its salt-binding behavior will first be explained. As reported in our preceding work, [Fe(bpyLac)₃]²⁺ showed unique 2-step binding profiles upon addition of chlorides (Fig. 6-b, gray symbols). These experiments revealed that anion (Cl⁻) and cation (Na⁺, K⁺, Ca²⁺, and Mg²⁺) bindings are responsible for the 1st and 2nd CD spectral responses, respectively (see our preceding paper for details).²⁶ It was also confirmed that the Lac appendages are responsible for the cation bindings.

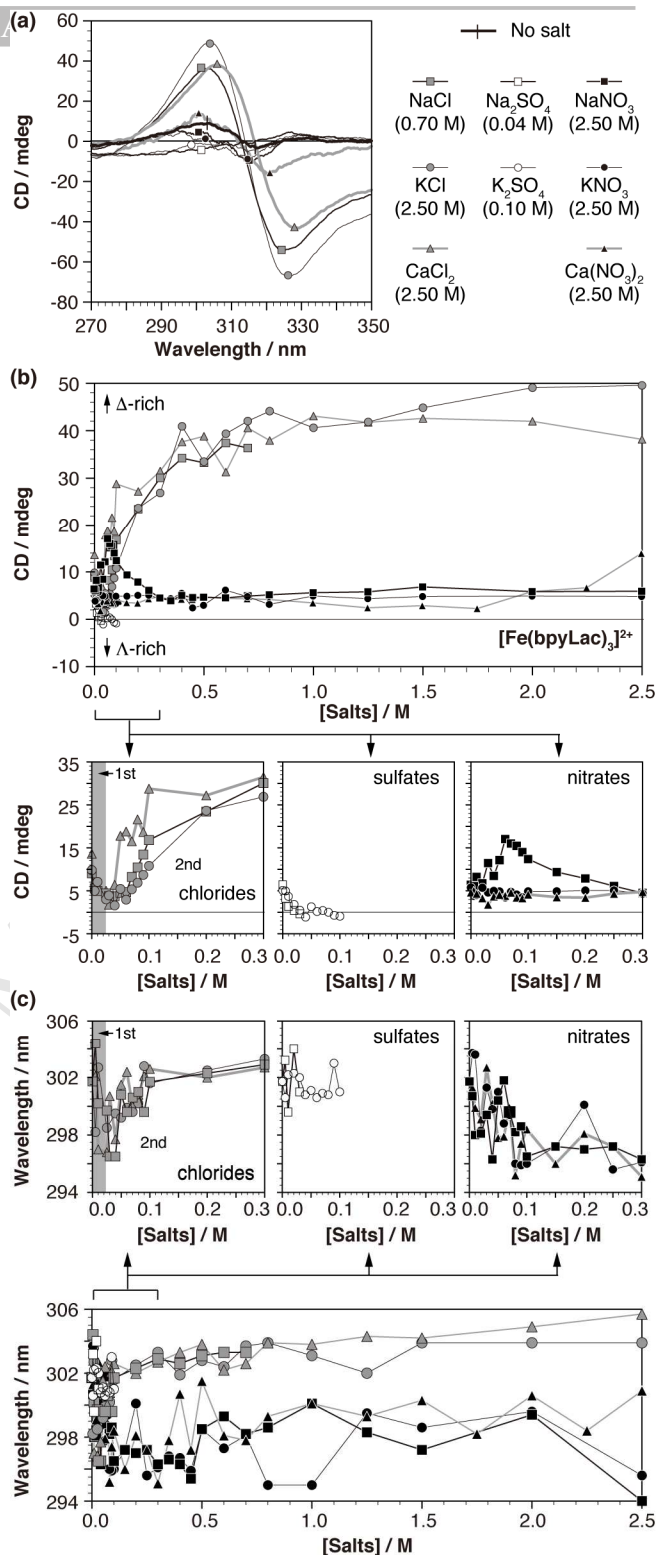


Fig. 6 (a) CD spectra of [Fe(bpyLac)₃]²⁺ with and without various salts, (b) plots of the peak intensity of the CD peak at the shorter wavelength (the left-most peaks in (a)) against salt concentration, and (c) wavelength of the CD peak at the shorter wavelength against salt concentration. [bpyLac] = 2.44 mM, [FeCl₂] = 7.33 mM, *d* = 0.2 mm, rt, in water.

Interestingly, the response of [Fe(bpyLac)₃]²⁺ to sulfate salts was quite unique; aqueous solutions of [Fe(bpyLac)₃]²⁺ became turbid upon addition of small amounts of sulfate salts (10 mM), with white precipitates observed. The white precipitates may suggest the dissociation of [Fe(bpyLac)₃]²⁺ to its precursor, bpyLac. In contrast, no such precipitation was observed upon the addition of chloride or nitrate salts. Furthermore, [Fe(bpyMal)₃]²⁺ and [Fe(bpyIma)₃]²⁺ did not give rise to any precipitates even

when subjected to much higher sulfate concentrations. These results clearly show that the dissociation of $[\text{Fe}(\text{bpyLac})_3]^{2+}$ arises from interactions between the Lac clusters and SO_4^{2-} . Due to the aggregation, the CD spectral responses of $[\text{Fe}(\text{bpyLac})_3]^{2+}$ were monitored only when sulfate salt concentrations were lower than 0.1 M. The positive-to-negative CD signal was slightly weakened upon addition of the sulfate salts (Fig. 6-b, white symbols).

The addition of nitrate salts also induced unique CD spectral responses in $[\text{Fe}(\text{bpyLac})_3]^{2+}$. For example, additions of small amounts of NaNO_3 greatly enhanced the signal intensity until the concentration reached 60 mM (Fig. 6-b, black square symbols). Further addition of NaNO_3 weakened the signal intensity until it was almost identical to that obtained in pure water ($[\text{NaNO}_3] = 300 \text{ mM}$). The enhanced CD signal observed in the presence of a specific range of nitrate salt concentrations (from 1 to 300 mM) was unique to NaNO_3 ; no such CD signal enhancement was induced by either KNO_3 nor $\text{Ca}(\text{NO}_3)_2$ (Fig. 6-b, black circles and triangles, respectively). These results indicate that simultaneous binding of both Na^+ and NO_3^- to $[\text{Fe}(\text{bpyLac})_3]^{2+}$ was achieved under certain NaNO_3 concentrations and such binding changed the flexible Lac packing into a rigid one suitable for the Δ - $[\text{Fe}(\text{bpy})_3]^{2+}$ core.

The addition of chloride and nitrate salts induced blue shifts of the CD signals. For example, the additions of small amounts of chloride salts ($\sim 30 \text{ mM}$) induced blue shifts of the positive CD signals from 302 to 298 nm, although further addition of chloride salts shifted the CD signals back to their original wavelengths obtained without any added salts (Fig. 6-c, gray symbols). The nitrate salts also induced similar blue shifts, but in contrast this blue shift was not reversed upon further addition of nitrate salts, even to much higher concentrations (Fig. 6-c, black symbols).

2.4.3. Salt-induced CD spectral changes of $[\text{Fe}(\text{bpyIma})_3]^{2+}$

In the absence of salts, $[\text{Fe}(\text{bpyIma})_3]^{2+}$ showed a CD signal with a negative-to-positive pattern, as measured from longer to shorter wavelengths, centered around 315 nm (Fig. 7-a, bold line). This CD signal was similar to those of both $[\text{Fe}(\text{bpyMal})_3]^{2+}$ and $[\text{Fe}(\text{bpyLac})_3]^{2+}$, indicating its flexible carbohydrate packings.

$[\text{Fe}(\text{bpyIma})_3]^{2+}$ exhibited salt-induced CD spectral changes that were entirely different from those of both $[\text{Fe}(\text{bpyMal})_3]^{2+}$ and $[\text{Fe}(\text{bpyLac})_3]^{2+}$. For example, in the case of chloride salts, the CD signal of $[\text{Fe}(\text{bpyIma})_3]^{2+}$ was almost unchanged until chloride salt concentrations reached $\sim 150 \text{ mM}$ (Fig. 7-b, gray symbols). However, when chloride salt concentrations were increased beyond 150 mM, the intensities of the CD signals weakened with increasing chloride salt concentrations. The CD signals finally inverted to the positive-to-negative patterns when chloride concentrations were above 300 mM (KCl and CaCl_2) or 600 mM (NaCl).

The nitrate and sulfate salts also induced CD spectral changes in $[\text{Fe}(\text{bpyIma})_3]^{2+}$. For example, additions of small amounts of nitrate salts clearly enhanced intensities of the CD signals, but such enhancements reached plateaus when nitrate concentrations reached $\sim 100 \text{ mM}$ (Fig. 7-b, black symbols). Again, the different cations of the different nitrate salts did not induce different CD spectral response of $[\text{Fe}(\text{bpyIma})_3]^{2+}$, indicating that NO_3^- is responsible for the CD spectral response. In the case of the sulfate salts (Na_2SO_4 and K_2SO_4), the CD signal of $[\text{Fe}(\text{bpyIma})_3]^{2+}$ remained almost unchanged until the sulfate salts concentrations reached $\sim 600 \text{ mM}$. Further addition of Na_2SO_4 entirely changed the CD response of $[\text{Fe}(\text{bpyIma})_3]^{2+}$, resulting in

the CD spectrum having a broad and positive CD signal centered at $\sim 320 \text{ nm}$.

In the case of $[\text{Fe}(\text{bpyIma})_3]^{2+}$, most salts did not induce any shift of its CD signal (Fig. 7-c). The one exception was Na_2SO_4 , which caused $[\text{Fe}(\text{bpyIma})_3]^{2+}$ to exhibit a CD spectrum that differed significantly from those of both Δ - and Λ - $[\text{Fe}(\text{bpy})_3]^{2+}$, at a concentration of 1.25 mM (Fig. 7-a, line with white square symbols).

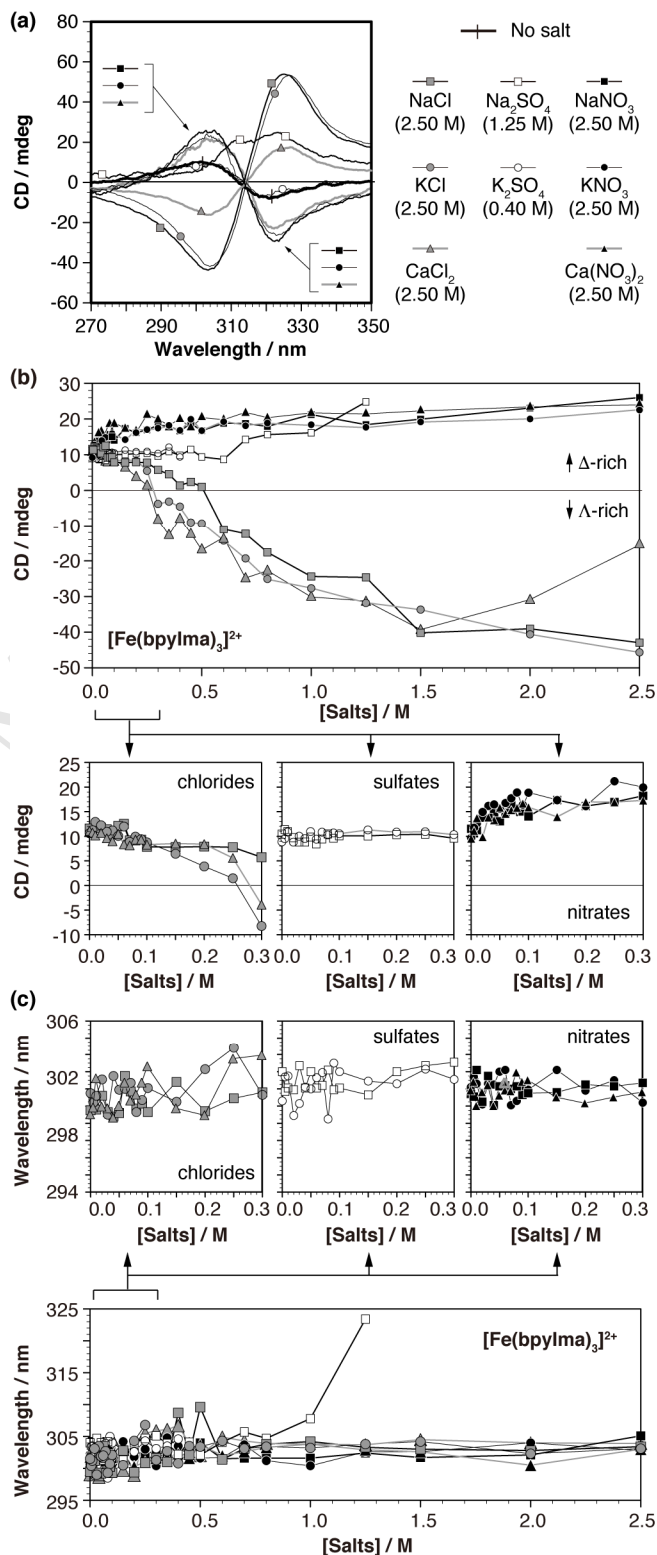


Fig. 7 (a) CD spectra of $[\text{Fe}(\text{bpyIma})_3]^{2+}$ with and without various salts, (b) plots of the peak intensity of the CD peak at the shorter wavelength (the left-most peaks in (a)) against salt concentration, and (c) wavelength of the CD peak at the shorter wavelength against salt concentration. $[\text{bpyIma}] = 2.44 \text{ mM}$, $[\text{FeCl}_2] = 7.33 \text{ mM}$, $d = 0.2 \text{ mm}$, rt, in water.

2.5. Additional experiments to reveal the mechanism behind the salt-induced CD spectral changes

So far, insufficient information has been discussed to allow clarification of the mechanism behind the salt-induced UV-vis spectral changes. However, the fact that these spectral changes mainly depended on the anions (Cl^- , NO_3^- , or SO_4^{2-}) demonstrated the substantial roles of the anions in the UV-vis spectral responses. It was assumed that the binding of the anions to the metalloglycoclusters would affect the conformation of the $[\text{Fe}(\text{bpy})_3]^{2+}$ cores, resulting in the UV-vis spectral response.

On the other hand, the CD spectral changes of the metalloglycoclusters clearly arose from the salt-induced conformational changes of their glycoclusters. Again, the CD spectral changes mainly depended on the anions, showing that the anions greatly affected the spatial carbohydrate packings of the glycoclusters. Only one exception was found in $[\text{Fe}(\text{bpyLac})_3]^{2+}$; it exhibit CD spectral response to both cations and anions.

Several experiments were conducted to reveal which parts of the metalloglycoclusters were responsible for the binding of the anions. One such experiment using $[\text{Fe}(\text{bpy})_3]^{2+}$ showed no UV-vis spectral changes under high concentrations of chloride, nitrate, or sulfate salts, indicating that the $[\text{Fe}(\text{bpy})_3]^{2+}$ cores do not have possible anion binding sites. Previously, we tried but failed to perform an experiment using tris-bpy ferrous complexes carrying glucoside (Glc) clusters or cellobioside (Cel) clusters to clarify the roles of carbohydrate appendages in the anion binding. Conversions of bpyGlc and bpyCel into the corresponding ferrous complexes ($[\text{Fe}(\text{bpyGlc})_3]^{2+}$ and $[\text{Fe}(\text{bpyCel})_3]^{2+}$, respectively) failed due to the insolubility of bpyGlc and bpyCel in water (see our preceding paper).²⁶ We also synthesized other bpy derivatives having amide linkages and phenyl spacers but no carbohydrate units in order to reveal the anion binding sites (Schemes S1 and S2). However, these bpy derivatives were also insoluble in water and thus their successful conversion into the corresponding $[\text{Fe}(\text{bpy})_3]^{2+}$ derivatives was not accomplished. We also tried to reveal the mechanism by which the anions induce the UV-vis spectral changes through ^1H NMR spectral analyses. The ^1H NMR spectra of the metalloglycoclusters were, however, quite broad and thus no informative clues were obtained.

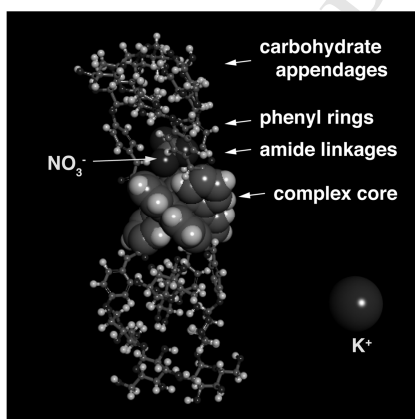


Fig. 8 The most stable conformation of Δ - $[\text{Fe}(\text{bpyMal})_3]^{2+}$ in co-existence with K^+ and NO_3^- during the MD simulation, in which only the complex core, K^+ and NO_3^- are presented in CPK models for clear presentation (See Fig. S5 for the colored version of this figure).

We were unable to obtain enough information to reveal the mechanism behind the salt-induced CD spectral changes through the aforementioned wet chemistries. Therefore, focus was shifted

to dry chemistries, including MD simulations, to reveal which parts of the metalloglycoclusters were responsible for the anion binding. For example, a MD simulation of Δ - $[\text{Fe}(\text{bpyMal})_3]^{2+}$ co-existing with K^+ and NO_3^- (Discovery Studio 4.5, CHARMm, $\epsilon = 80$, 10 ps equilibrium, 90 ps dynamics) indicated that the most stable conformation of Δ - $[\text{Fe}(\text{bpyMal})_3]^{2+}$ captured NO_3^- via hydrogen bonding with its amide linkages. On the contrary, K^+ was positioned away from Δ - $[\text{Fe}(\text{bpyMal})_3]^{2+}$ during the MD simulation, showing their low affinity for one another. The data obtained through the MD simulations suggest the amide linkages as possible anion-binding sites.

2.6. Salt-induced changes in rheological properties of solutions of the aqueous metalloglycoclusters

During the previously described experiments, it was noticed that some metalloglycocluster solutions became viscous upon the addition of certain salts. Unfortunately, the typical experiments for assessing the rheological properties of solutions include viscosity measurements, which usually require large sample volumes (~ 10 mL) and thus this method was not appropriate for our metalloglycocluster solutions (~ 100 μL). Instead, an experiment to assess the rheological properties of the aqueous metalloglycocluster solutions was performed as follows. Briefly, the aqueous metalloglycocluster solutions were slowly expelled from a syringe with a needle, and drops were weighed as they fell from the point of the needle.

As shown in Fig. 9, changes in the weight of each drop were negligible when salts were added to aqueous solutions of $[\text{Fe}(\text{bpyMal})_3]^{2+}$ or $[\text{Fe}(\text{bpyIma})_3]^{2+}$. On the other hand, the weight per drop of the aqueous $[\text{Fe}(\text{bpyLac})_3]^{2+}$ solution increased, specifically upon addition of sulfate salts. In addition, K_2SO_4 and Na_2SO_4 elicited different impacts on the weight per drop; the former increased the weight of each drop more significantly than the latter. This finding is quite interesting since it indicates that not only SO_4^{2-} , but also the cations (Na^+ and K^+) affected the rheological properties of the metalloglycocluster solutions, specifically for that having Lac appendages.

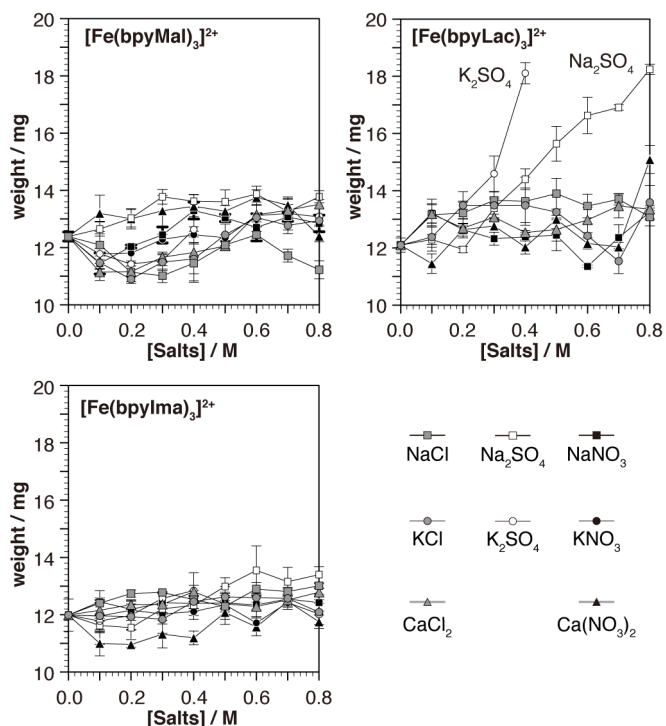


Fig. 9 Plots of the weight per drop of the aqueous metalloglycocluster solutions against the concentration of the co-existing salts. $[\text{bpyMal}]$, $[\text{bpyLac}]$, or $[\text{bpyIma}] = 2.44$ mM, $[\text{FeCl}_2] = 7.33$ mM, $n = 3$, rt, in water.

3. Conclusions

We developed $[\text{Fe}(\text{bpy})_3]^{2+}$ derivatives having six carbohydrate appendages as molecular mimics of cell surface glycoclusters. Using these metalloglycoclusters, the spatial carbohydrate packing within the glycoclusters was assessed through UV-vis and CD spectral analyses, revealing that they contained flexible carbohydrate packings in pure water.

In the presence of various salts, the spatial carbohydrate packings changed, mainly in anion-dependent manners. The anion-dependent conformational changes were well-demonstrated in $[\text{Fe}(\text{bpyMal})_3]^{2+}$ and $[\text{Fe}(\text{bpyIma})_3]^{2+}$. This anion-dependency was in clear contrast to the anion- and cation-dependent conformational changes induced in $[\text{Fe}(\text{bpyLac})_3]^{2+}$. In addition, it was found that the addition of sulfate salts changed the rheological properties of an aqueous solution of $[\text{Fe}(\text{bpyLac})_3]^{2+}$. These results may indicate that the salt-induced conformational changes are linked to CCIs between the metalloglycoclusters. However, this assumption requires further discussion, since partial dissociation of $[\text{Fe}(\text{bpyLac})_3]^{2+}$ was also observed upon addition of these sulfate salts.

Altogether, the results indicate that the conformations of the glycoclusters change upon addition of numerous salts, and that carbohydrate packing may play an important role in inducing CCIs. In studies of CCIs the ions (Ca^{2+} in many cases) have been thought of as molecular glues which connect two carbohydrate units. The formation of multiple carbohydrate-ion-carbohydrate complexes has been thus assumed, without clear evidence, as a main driving force for the induction of CCIs. Based on these proposed mechanisms, no attention has been paid to the ion-induced conformational changes in the glycoclusters. However, the findings in this paper suggest an alternative mechanism, specifically that the ions change the carbohydrate packing in glycoclusters into those more suitable for CCIs.

Although the synthesized metalloglycoclusters offered useful insights into the spatial carbohydrate packing in the glycoclusters and their salt-induced conformational changes, their chemical structures differ from those of the natural GSLs on cell surfaces. Specifically, the spacer units tethering the carbohydrate units to the $[\text{Fe}(\text{bpy})_3]^{2+}$ cores are phenyl rings in the synthesized metalloglycoclusters, which are clearly different from the spacer units tethering the carbohydrate units to the hydrophobic tails in natural GSLs. Currently, new metalloglycoclusters having L-serine as the spacer units are under development in our group to better mimic the natural glycoclusters on cell surfaces and allow evaluation of the effect of the ions on their spatial carbohydrate packings.

4. Experimental Section

4.1. General

^1H and ^{13}C NMR spectra were acquired on a JEOL AL300 spectrometer (JEOL Resonance, Ltd., Japan) in CDCl_3 , D_2O , or $\text{DMSO}-d_6$. Chemical shifts were reported in ppm (δ) relative to TMS or internal references such as HOD. Matrix-assisted laser desorption ionization time-of-flight (MALDI-TOF) mass spectra were recorded on a SHIMAZU AXIMA-CFR+ (SHIMAZU, Ltd., Japan) or SHIMAZU AXIMA-Confidence (SHIMAZU, Ltd., Japan). IR spectra were recorded on a JASCO FT/IR-4100 Fourier transform infrared spectrometer (JASCO Co., Ltd., Japan). UV-vis spectra were recorded on a V-630 UV-visible spectrophotometer (JASCO Co., Ltd., Japan). Circular dichroism (CD) spectra were acquired on a JASCO J-820 spectropolarimeter (JASCO Co., Ltd., Japan). Silica gel 60 N

(spherical, neutral, particle size 63–210 μm) for column chromatography was purchased from Kanto Chemical Co., Inc., Japan. Thin layer chromatography (TLC) was carried out with Whatman TLC glass plates (Partisil[®] K6F) pre-coated with silica gel (60 \AA) with a fluorescent indicator ($\lambda = 254 \text{ nm}$). All other chemicals were purchased from Wako Pure Chemicals Co., Ltd., Japan, Kishida Chemicals Co., Ltd., Japan, GODO Co., Japan, or Kanto Chemical Co., Inc., Japan, and used without further purification.

4.2. 2,2'-Bipyridine-5,5'-dicarboxyl chloride

To 2,2-bipyridine-5,5'-dicarboxylic acid, thionyl chloride was added and then, the resultant heterogeneous mixture was refluxed with magnetic stirring until it became homogeneous (ca. 5 h). The resultant reaction mixture was evaporated to dryness and dried in vacuo to afford the title compound as a pale-yellow powder. The product was then used for the synthesis of bpyLacAc, bpyMalAc, bpyIma, bpyPhe, or bpyPhe(OC_2H_4)₂OH without any purification and characterization. The amounts of 2,2-bipyridine-5,5'-dicarboxylic acid and thionyl chloride used to synthesize each of the bpy derivatives were reported in its synthetic procedure.

4.3. 1,2,3,4,2',3',4',6'-hexa-O-acetyl-isomaltose (AcIma, 1)

To isomaltose (0.61 g) in pyridine (100 ml), acetic anhydride (50 ml) was added and the resultant mixture was stirred at ambient temperature for overnight. The resultant mixture was poured into ice and diluted with ethyl acetate. The organic layer was then washed with 0.5 N HCl aq. and saturated NaHCO_3 aq. repeatedly. The organic layer was dried over anhydrous MgSO_4 , filtered, evaporated and dried in vacuo to give 1.21 of the titled compound (AcIma) as white powder. The compound was used as a substrate in the following section without any purification/identification process.

4.4. 2,3,4,2',3',4',6'-hexa-O-acetyl-isomaltosyl bromide (AcImaBr, 2)

To AcIma in CH_2Cl_2 (20 ml), acetic anhydride (6 ml) and hydrogen bromide in acetic acid (30%, 20 ml) were added and the resultant mixture was stirred at ambient temperature for 2.5 h. The resultant mixture was poured into ice and diluted with ethyl acetate. The organic layer was washed with saturated NaHCO_3 aq. repeatedly. The organic layer was then dried over anhydrous MgSO_4 , filtered, evaporated, dried in vacuo and used as a substrate of the following reaction without any purification/identification process.

4.5. 1-(*p*-Nitrophenyl)-2,3,4,2',3',4',6'-hexa-O-acetyl-isomaltoside (pNPIma, 3)

To AcImaBr and sodium *p*-nitrophenoxide (1.12 g) in dry acetone (150 ml) was stirred at 75 $^\circ\text{C}$ for overnight. The resultant mixture was diluted with ethyl acetate and the resultant organic layer was washed with NaCl aq. repeatedly. The organic layer was then dried over anhydrous MgSO_4 , filtered, evaporated and dried in vacuo. The residue was then subjected to purification on silica-gel (toluene/AcOEt = 5/1 to 1/2, v/v) to give the titled compound (pNPIma) as white powder; ^1H NMR (300 MHz, CDCl_3) δ 8.33 (d, $J = 9.3 \text{ Hz}$, 2H), 7.15 (d, $J = 9.0 \text{ Hz}$, 2H), 5.49 (t, $J = 9.9 \text{ Hz}$, 1H), 5.36 (t, $J = 9.0 \text{ Hz}$, 1H), 5.31–5.20 (m, 2H), 5.09–5.00 (m, 3H), 4.88 (dd, $J = 3.6, 10.2 \text{ Hz}$, 1H), 4.08 (dd, $J = 4.5, 12.6 \text{ Hz}$, 1H), 4.04–3.79 (m, 4H), 3.53 (dd, $J = 1.8, 9.6 \text{ Hz}$, 2H), 2.12 (s, 3H), 2.10 (s, 3H), 2.08 (s, 3H), 2.07 (s, 3H), 2.06 (s, 3H), 2.06 (s, 3H), 1.81 (s, 3H); ^{13}C NMR (75 MHz, CDCl_3) δ 170.5, 170.2, 170.1, 170.1, 169.5, 169.4, 169.2, 161.3, 143.3, 126.2, 116.4, 98.1, 95.6, 73.3, 72.4, 70.9, 70.7, 69.5, 68.7, 68.3,

67.9, 67.6, 66.4, 61.5, 20.8, 20.7, 20.7, 20.6, 20.6, 20.1; FT-IR (KBr, cm^{-1}): 1755, 1554, 1522, 1370, 1346, 1234, 1038. MALDI-TOF-MS, $[\text{M}+\text{Na}]^+ = 780.19$ (calc. 780.21).

4.6. 1-(*p*-Aminophenyl)-2,3,4,2',3',4',6'-hexa-*O*-acetyl-isomaltoside

To *p*NPIma in THF (70 ml), Pd/C (0.42 mg) was added and the resultant mixture was vigorously stirred under H_2 atmosphere at ambient temperature for overnight. The resultant mixture was filtrated through a celite pad and the filtrate was evaporated and dried in vacuo. The residue was then subjected to purification on silica-gel ($\text{CHCl}_3/\text{MeOH} = 50/1$, v/v) to give the titled compound (*p*APIma) as white powder. This compound was used in the following reaction without $^1\text{H}/^{13}\text{C}$ NMR, MS and IR spectral characterizations.

4.7. 5,5'-Bis(-*N*-(*p*-*O*-(2,3,6,2,3,4,6-hepta-*O*-acetyl- β -isomaltosyl)phenyl)-aminocarbonyl)-2,2'-bipyridine (*bpyImaAc*)

To *p*APIma (0.37 g, 0.51 mmol) and Et_3N (2 ml) in THF (65 ml), *bpyCOCl* prepared from 28 mg (0.11 mmol) of *bpyCOOH* in THF (5.0 ml) was added and then, the resultant mixture was stirred at the ambient temperature for 20 min. The resultant reaction mixture was poured into iced water and diluted with ethyl acetate. The organic layer was then washed with 0.5 N HCl aq. and NaHCO_3 saturated aqueous solution repeatedly. The organic layer was dried over anhydrous Na_2SO_4 , filtered, and evaporated to give pale yellow syrup. The resultant syrup was then subjected to silica-gel column chromatographic purification process (hexane only ~ hexane/ $\text{AcOEt} = 1:9$, gradient) to give the titled compound (116 mg) in 61% yield (from *bpyCOOH*) as a pale yellow powder.; ^1H NMR (300 MHz, CDCl_3) δ 9.24 (d, $J = 1.8$ Hz, 2H), 8.70 (s, 2H), 8.58 (d, $J = 8.4$ Hz, 2H), 8.37 (dd, $J = 2.1$, 8.4 Hz, 2H), 7.76 (d, $J = 9.0$ Hz, 4H), 7.06 (d, $J = 8.7$ Hz, 4H), 5.41 (t, $J = 9.6$ Hz, 2H), 5.34 (t, $J = 9.0$ Hz, 2H), 5.25 (t, $J = 9.7$ Hz, 2H), 5.12–4.97 (m, 8H), 4.90 (dd, $J = 3.9$, 9.9 Hz, 2H), 4.19–4.14 (m, 2H), 4.01–3.76 (m, 8H), 3.48 (d, $J = 9.6$ Hz, 2H), 1.84 (s, 6H). ^{13}C NMR (75 MHz, CDCl_3) δ 170.398, 170.357, 170.160, 170.094, 169.815, 169.675, 169.165, 163.649, 157.476, 153.974, 148.005, 136.085, 132.953, 130.684, 122.11, 121.420, 117.761, 101.147, 99.142, 76.198, 72.868, 72.548, 71.479, 70.953, 70.764, 69.111, 66.612, 62.017, 60.817, 20.831, 20.724, 20.659, 20.527. FT-IR (KBr, cm^{-1}): 1754, 1509, 1370, 1224, 1038. MALDI-TOF-MS, $[\text{M}+\text{Na}]^+ = 1685.37$ (calc. 1685.49).

4.8. 5,5'-Bis(-*N*-(*p*-*O*-(β -isomaltosyl)phenyl)-aminocarbonyl)-2,2'-bipyridine (*bpyIma*)

To *bpyImaAc* (0.67 g, 0.40 mmol) in methanol/THF (1:1, 50 ml), aqueous ammonia was added dropwise until pH value of the resultant mixture became larger than 10. The resultant reaction mixture was stirred at ambient temperature for overnight. After confirming that the pH value of the reaction mixture was still larger than 10, the resultant mixture was concentrated to form white precipitate. The precipitate was retrieved through filtration and dried over filter paper overnight to give the title compound as a white powder (0.37 g, >99 %); d_{H} (300 MHz, $\text{DMF-}d_7 + \text{D}_2\text{O}$): 9.11 (t, J 1.5 Hz, 2H), 8.23 (d, J 1.5 Hz, 2H), 7.61 (d, J 9.0 Hz, 4H), 6.94 (d, J 9.0 Hz, 4H), 4.66 (d, J 7.8 Hz, 2H), 4.58 (d, J 3.9 Hz, 2H), 3.64–3.01 (m, 24H); d_{C} (75 MHz, $\text{DMF-}d_7 + \text{D}_2\text{O}$): 162.9, 162.0, 156.2, 153.8, 148.2, 136.0, 132.6, 130.528, 121.2, 120.0, 116.2, 100.9, 98.2, 76.4, 74.5, 73.2, 73.1, 72.1, 71.8, 70.0, 79.8, 66.0, 60.7; HR-ESI-TOF-MS, $[\text{M}+\text{H}]^+ = 1075.3550$ (calc. 1075.3519); n_{max} (KBr) 3375, 1647, 1542, 1508, 1417, 1224, 1078 cm^{-1} .

4.9. UV-vis and CD spectroscopy titration experiments

Before the titration experiments, we prepared the aqueous metalloglycocluster solutions and the aqueous salt solutions as the stock solutions. In the case of the former, we mixed the glycobpys and FeCl_2 in water to prepare the aqueous metalloglycocluster solutions ($[\text{bpyMal}]$, $[\text{bpyLac}]$, or $[\text{bpyIma}] = 24.4$ mM, $[\text{FeCl}_2] = 73.3$ mM). We then mixed the metalloglycocluster solutions (3 μl), aqueous salt solutions (0–27 μl), and pure water (27–0 μl) to prepare the sample solutions (30 μl) for the spectroscopy titration assays. After the incubation of these sample solutions for 1-day, their UV-vis and CD spectra were measured by using a V-630 UV-visible spectrophotometer and a JASCO J-820 spectropolarimeter equipped with SAH-769 and MSD-462, respectively.

4.10. MD simulations

Before the MD simulation of the molecular assembly consisting of Λ - $[\text{Fe}(\text{bpyMal})_3]^{2+}$, K^+ , and NO_3^- , we built a Λ - $[\text{Fe}(\text{bpyMal})_3]^{2+}$ with a stable conformation through a molecular mechanics (MM) calculation. Briefly, we constructed a Λ - $[\text{Fe}(\text{bpy})_3]^{2+}$ and then, its stable conformation was obtained through its MM calculation. After the construction of Λ - $[\text{Fe}(\text{bpy})_3]^{2+}$, the spatial positions of all atoms in its structure were fixed. This spatial fixing was essential to successfully achieve the MD simulation on the three-component molecular assembly, since CHARMM force field was not suitable for molecules having Fe-N bonds. We then attached β -maltosyloxyphenylaminocarbonyl ($\text{Mal}\beta\text{PheNHCO-}$) units onto all C5 positions of the pyridine (py) units of Λ - $[\text{Fe}(\text{bpy})_3]^{2+}$ and constructed Λ - $[\text{Fe}(\text{bpyMal})_3]^{2+}$ with *E* and *Z* configurations about its $\text{C}_{5\text{py}}\text{-C}_{\text{C=O}}$ bonds and amide bonds, respectively. We then added K^+ and NO_3^- ions nearby the trivalent Mal clusters of Λ - $[\text{Fe}(\text{bpyMal})_3]^{2+}$ to obtain the three-component molecular assembly consisting of Λ - $[\text{Fe}(\text{bpyMal})_3]^{2+}$, K^+ and NO_3^- . Before starting the MD simulation, we applied distance restrictions ($\text{Fe}^{2+}\text{-K}^+$ and $\text{Fe}^{2+}\text{-NO}_3^-$) to this three-component molecular assembly so that the ions (K^+ and NO_3^-) did not leave from Λ - $[\text{Fe}(\text{bpyMal})_3]^{2+}$. The subsequent MD simulation (CHARMM, $\epsilon = 80$, 10 ps equilibrium, 90 ps dynamics) gave the most stable conformation of the three-component molecular assembly (Fig. 8).

4.11. Dropping test of metalloglycocluster solutions

According to the procedure described in section 4.9, we prepared the aqueous metalloglycocluster solutions containing varying concentrations of the chloride, nitrate, or sulfate salts. After the 1-day incubation at ambient temperature, these solutions were slowly expelled from a plastic syringe (Tuberculin syringe, SS-01T, TERUMO Co., Japan) with a needle whose outer and inner diameters were 0.72 and 0.41 mm, respectively. The drops were weighed as they fell from the point of the needle.

Declaration of interest

Declarations of interest: none

Acknowledgements

This work was supported by Grant-in-Aid for Scientific Research (No. 25810105) from the Ministry of Education, Culture, Sports, Science and Technology, Japan and Special Research Fund of Toyo University.

References and notes

- Hirohashi N, Kamei N, Kubo H, Sawada H, Matsumoto M, Hoshi M. *Dev. Growth Differ.* 2008;50:S221–S238.
- Schengrund CL. *Trends Biochem. Sci.* 2015;40:397–406.

3. Nakayama H, Ogawa H, Takamori K, Iwabuchi K. *Arch. Immunol. Ther. Exp.* 2013;61:217–228.
4. Fenderson BA, Eddy EM, Hakomori S. *BioEssays* 1990;12:173–179.
5. Hakomori S. *Pure Appl. Chem.* 1991;63:473–482.
6. Iwabuchi K, Yamamura S, Prinetti A, Handa K, Hakomori S. *J. Biol. Chem.* 1998;273:9130–9138.
7. Delbianco M, Bharate P, Varela-Aramburu S, Seeberger PH. *Chem. Rev.* 2016;116:1693–1752.
8. Matsuura K, Kobayashi K. *Glycoconjugate J.* 2004;21:139–148.
9. Hasegawa T, Sasaki T. *Chem. Commun.* 2003;8:978–979.
10. Altamore TM, Fernández-García C, Gordon AH, Hübscher T, Promsawan N, Ryadnov MG, Doig AJ, Woolfson DN, Gallagher T. *Angew. Chem. Int. Ed.* 2011;50:11167–11171.
11. Simpson GL, Gordon AH, Lindsay DM, Promsawan N, Crump MP, Mulholland K, Hayter BR, Gallagher T. *J. Am. Chem. Soc.* 2006;128:10638–10639.
12. Bavireddi H, Bharate P, Kikkeri R. *Chem. Commun.* 2013;49:3988–3990.
13. Lorentz B, de Cienfuegos LÁ, Oelkers M, Krienmen E, Brand C, Stephan M, Sunnick E, Yüksel D, Kalsani V, Kumar K, Werz DB, Janshoff A. *J. Am. Chem. Soc.* 2012;134:3326–3329.
14. Kunze A, Bally M, Hoeoek F, Larson G. *Sci. Rep.* 2013;3:1452–1459.
15. Jayaraman N, Maiti K, Naresh K. *Chem. Soc. Rev.* 2013;42:4640–4656.
16. de la Fuente, JM, Eaton P, Barrientos AG, Menéndez M, Penadés S. *J. Am. Chem. Soc.* 2005;127:6192–6197.
17. Reynolds AJ, Haines AH, Russell DA. *Langmuir* 2006;22:1156–1163.
18. Zhao J, Liu Y, Park HJ, Boggs JM, Basu A. *Bioconjugate Chem.* 2012;23:1166–1173.
19. Seah N, Santacrose PV, Basu A. *Org. Lett.* 2009;11:559–562.
20. Chen Q, Cui Y, Zhang TL, Cao J, Han BH. *Biomacromolecules*, 2010;11:13–19.
21. Lai CH, Hütter J, Hsu CW, Tanaka H, Varela-Aramburu A, Cola LD, Lepenies B, Seeberger PH. *Nano Lett.* 2016;16:807–811.
22. Vilanova E, Santos GRC, Aquino RS, Valle-Delgado JJ, Anselmetti D, Fernández-Busquets X, and Mourão PAS. *J. Biol. Chem.* 2016;291:9425–9437.
23. Otsuka A, Sakurai K, Hasegawa T. *Chem. Commun.* 2009;36:5442–5444.
24. Iwamura M, Koyama R, Nonaka T, Dai F, Matsuoka R, Nakamura M, Iwabuchi H, Okada T, Hasegawa T. *Bull. Chem. Soc. Jpn.* 2016;89:617–625.
25. Nakamura M, Tsutsumi M, Ishikawa Y, Umemiya H, Hasegawa T, Izawa K, Abe H, Togashi Y, Kinone T, Sekiguchi S, Igumi M, Ide K, Hasegawa T. *Tetrahedron* 2013;69:3019–3026.
26. Nonaka Y, Uruno R, Dai F, Matsuoka R, Nakamura M, Iwamura M, Iwabuchi H, Okada T, Chigira N, Amano Y, Hasegawa T. *Tetrahedron* 2016;72:5456–5464.
27. Milder SJ, Gold JS, Kliger DS. *J. Am. Chem. Soc.* 1986;108:8295–8296.

Supplementary Materials

Supplementary data related to this article containing length of each side of the triangles whose corners are occupied by C4 atoms of the non-reducing carbohydrate terminals (Fig. S1), schematic illustration of our metalloglycoclusters for investigating stable carbohydrate packings (Fig. S2), a colored version of Fig. 1 (Fig. S3), representative UV-vis spectral changes of the metalloglycoclusters (Fig. S4), a colored version of Fig. 8 (Fig. S5), synthetic routes to access the bpy derivatives (Schemes S1 and S2), and $^1\text{H}/^{13}\text{C}$ NMR spectra of the newly synthesized compounds in this paper are available online free of charge.

